J Mater Sci (2015) 50:3994–4002
DOI 10.1007/s10853-015-8956-6

Grain size evolution in Cu-based shape memory alloys

S. Montecinos[1,2] · A. Cuniberti[1,2] · R. Romero[1,3] · M. Stipcich[1,2]

Received: 4 December 2014 / Accepted: 5 March 2015 / Published online: 13 March 2015

Abstract A study of the grain growth kinetics in two shape memory alloys, CuAlBe and CuZnAl, is reported. Isothermal aging treatments at temperatures between 1023 and 1123 K were conducted, determining the grain size distribution as a function of time. The results show that the size distribution can be described by a log-normal type relationship, and is time-invariant. It was found that the arithmetic mean grain size almost coincide with the mode, which means that it is a representative parameter of the microstructure along the annealing time. The growth kinetics is strongly dependent on the aging temperature in CuZnAl, while is weakly in CuAlBe. It was verified that the grain size-time power law usually applied is not appropriate to describe the process, and an early departure from the ideal behavior is observed. The modification with a time-dependent dragging force gives a reasonable approximation to the grain growth kinetic. The obtained results are compared with the scarce data existing on this type of alloys.

✉ S. Montecinos
dmonteci@exa.unicen.edu.ar

A. Cuniberti
adelac@exa.unicen.edu.ar

R. Romero
rromero@exa.unicen.edu.ar

M. Stipcich
mstipci@exa.unicen.edu.ar

[1] Instituto de Física de Materiales Tandil-IFIMAT, Facultad de Ciencias Exactas, Universidad Nacional del Centro de la Provincia de Buenos Aires, Pinto 399, 7000 Tandil, Argentina

[2] CONICET, Provincia de Buenos Aires, Argentina

[3] CICPBA, La Plata, Provincia de Buenos Aires, Argentina

Introduction

Shape memory alloys (SMA) are able to show high damping capacity, making them good candidates for vibration isolation both in an active and passive manner. Cu-based SMA are commercially attractive due to their low cost and interesting properties when vibration isolation and suppression is required in engineering applications, from isolation platforms for sensitive experimentation and manufacturing to stabilization of large space structures [1].

The metastable β phase in Cu-based SMA transforms martensitically under appropriate temperature and mechanical stress conditions. This transformation is responsible for the shape memory effect, pseudoelasticity, and changes of mechanical properties with temperature, providing the material's damping potential [2–5]. The critical temperature as well as the critical stress for the martensitic transformation start is strongly dependent on the chemical composition. The martensitic transformation is also affected by the microstructural state, particularly by the presence of lattice defects [6–9], and the grain size plays an important role in polycrystalline specimens [10–15]. Large grains require higher values of strain associated to the transformation. This distortion is partially compensated by the generation of martensite variants, but also is supported by the grain boundary, leading sometimes to disintegration of material. Intergranular cracking, which limits many potential applications, is observed especially in CuAlNi and CuZnAl alloys [2]. As the grain size increases, the critical applied stress to start the martensitic transformation decreases, following a Hall–Petch relation type in β CuAlBe [16] and CuAlMn alloys [17]. This relationship has been also reported in martensitic CuAl [18] and CuZnAl alloys [19]. In CuAlBe and CuZnAl alloys, the largest transformation strain is obtained in well-oriented single

crystals, and smaller values are obtained in polycrystals due to the different degrees of transformation between different grains [11, 20]. We have performed detailed studies about the thermomechanical and pseudoelastic behavior product of the martensitic transformation induced by tensile and compressive tests of CuAlBe polycrystals [5, 10, 11, 16, 21]. The recoverable pseudoelastic strain increases and the stress hysteresis decreases as the grain size increases [16, 21]. High damping capacities with values near to those reported for NiTi alloys under similar conditions can be obtained [5].

The knowledge of the grain ensemble evolution when the material is heat treated at temperatures in the range of the β phase stability is of central importance due to its strong influence on the martensitic transformation and associated effects. Although grain growth can be inhibited by the addition of refiners, the study of grain growth in the alloy without refiners would be the first step.

The purpose of the present work is to report a detailed study of the grain ensemble evolution in two SMA, CuAlBe and CuZnAl, subjected to thermal treatments (TT) at 1023, 1073, and 1123 K. It must be mentioned that no similar studies on CuAlBe alloys have been reported. Samples at temperatures 1023–1123 K are well in the β-phase stability field, avoiding the precipitation of the stable phases α and/or γ. The obtained results are compared with the scarce data about grain growth behavior of this type of alloys available in the literature [22–24].

Materials and methods

A Cu-11.41Al-0.50Be (wt%) commercial alloy was used (CAB). It was provided by TREFIMETAUX, France, as hot extruded bars with 5.1 mm diameter. The chemical composition was checked by atomic absorption spectrophotometry. Grains exhibit similar appearance in the longitudinal and transversal faces in the as-received bars. Then, cross-section disks with 1–2 mm thickness were obtained. A Cu-16.63Zn–8.03Al (wt%) alloy (CZA) was prepared by melting the material in a sealed quarts capsule under partial Ar atmosphere, followed by quenching in water at room temperature. The obtained ingot, with 20 mm diameter and 50 mm length, was subjected to a homogenization heat treatment at 1073 K during 24 h (details are described in [25]). The grain size appeared similar in the longitudinal and transversal direction, and cross-section disks of around 20 mm diameter and 5 mm thickness were cut. Both alloys were in β phase at room temperature (RT). The martensitic transition temperature Ms is around 253 K in the CAB, and 265 K in the CZA.

The samples were subjected to heat treatments for different times in a resistance furnace, at 1023, 1073, and 1123 K, and water quenched at RT. The temperature control in the furnace was assured within ± 2 K. Then, the samples were smoothed with 1000 grit emery paper and prepared to reveal grain boundaries:

- *CAB* electropolished with a solution of chromium trioxide in phosphoric acid at ~ 4 V. Then, in order to reveal the grain boundaries, the samples were suspended in a solution of ferric chloride.
- *CZA* chemically etched by immersion in a solution of 10 % HNO_3 in H_2O during ≈ 20 s.

Mean grain sizes were determined from micrographs obtained by optical microscopy at RT, using two procedures on at least three micrographs of each sample:

(a) Using the intercept line method.
(b) Measuring the area of each grain using the software Image Tool 3.0 and estimating an equivalent diameter considering them with circular form.

Then, an average diameter was obtained.

Results

The microstructure of the CAB as-received bar appears as completely recrystallized. No columnar grains in the extrusion direction are observed but instead equiaxed grains with similar appearance in the longitudinal and transversal faces. Grains in the CZA ingots were roughly equiaxed, with similar size in the longitudinal and transversal faces.

Figure 1a and b shows the samples cross-section of the CAB alloy and the CZA alloy, respectively, previous to the annealing treatments. The measured initial average grain size, D_0, is (0.050 ± 0.002) mm for the CAB, and (1.47 ± 0.09) mm for the CZA. The different manufacturing routes for both alloys are reflected in the notable initial grain size disparity.

The average grain sizes, D, determined as the arithmetic mean, as a function of annealing time are shown in Fig. 2 for both alloys. As general behavior, it can be observed that after a short time, the grain size increases very fast in a first stage, then the growth rate decreases and the grain size reaches a saturation value, D_{max}, at long annealing times. It is worth mentioning that a saturation grain size has also been reported for CuZn, CuZnAl, and CuAlNi SMA [22]. The grain growth occurs homogeneously over the whole sample in both alloys. As the aging temperature increases, higher grain sizes at shorter times are reached, which is more notable for the CZA alloy. The CAB behavior is less sensitive to the annealing temperature than the CZA. The maximum grain size, D_{max}, is slightly dependent on the annealing temperature, around 1.2 mm in the CAB and 2.1 mm in the CZA. It is equivalent to a ratio D_{max}/disk

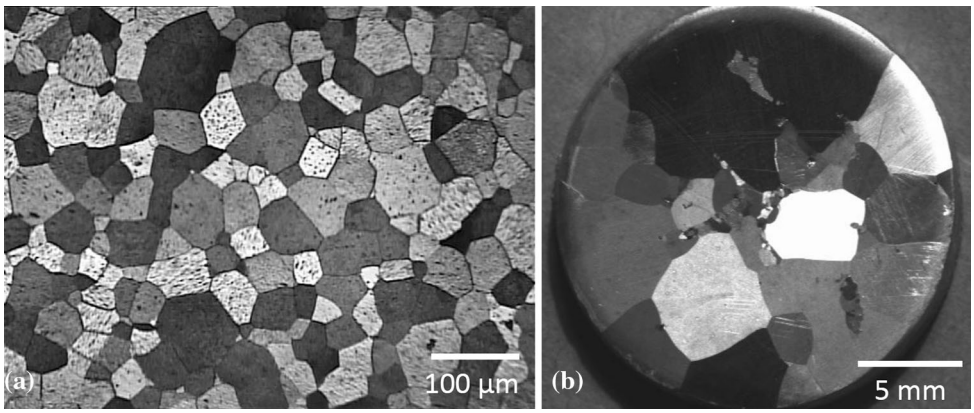

Fig. 1 Micrographs of representative samples before annealing treatments of: **a** CAB alloy, and **b** CZA alloy

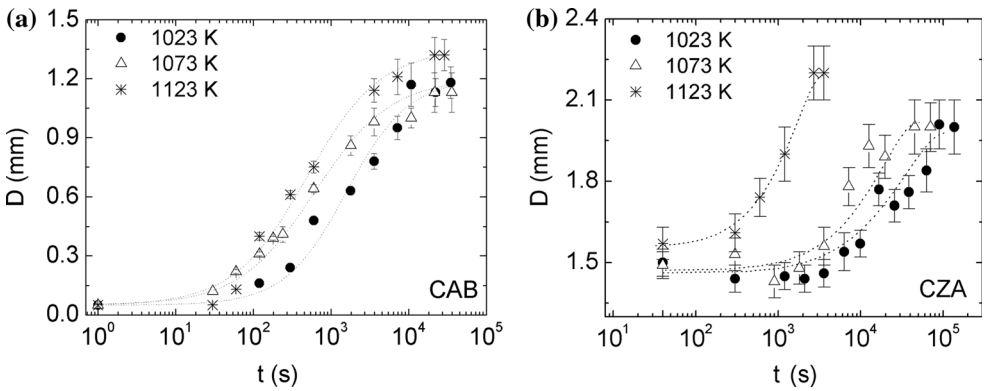

Fig. 2 Average grain size against annealing time at different temperatures for CAB (**a**), and CZA (**b**)

diameter of almost 4 in the CAB sample, and 10 in the CZA sample.

It must be mentioned that the annealing temperatures are higher than that corresponding to the β phase ordered state field. The CuZnAl alloys suffer two order transformations under heating, $L2_1 \rightarrow B2$ at around 635 K, and $B2 \rightarrow A2$ (disordered) at around 811 K for the studied composition [26]. The CuAlBe alloys suffer one order transformation under heating, $DO_3 \rightarrow A2$ at around 800 K for the studied composition [27]. Then, the grain growth proceeds in the disordered state (A2 phase) during the heat treatments.

It is well known that grains have not the same size, even in a so-called uniform grain structure. The grain size distribution was analyzed throughout the grain growth process, in more detail for the CAB. At least three micrographs of different samples in each annealing condition were used for grain size measurements. The initial sampling was made with the area measurement of around 250 grains; the sampling size was smaller with the annealing progress, with a minimum of around 20 grain area determinations. Although the empirical distributions are hampered for long time annealing by the low statistics, the fitting procedure gives suitable results. Representative micrographs showing the grain structure after different annealing times are presented in Fig. 3. Figure 4 shows the obtained grain size distributions for selected annealing times, normalized by the corresponding arithmetic mean grain size, *d/D*. It can be seen that the distributions maintain a unimodal shape, and remain invariant or isomorphic as the annealing proceeds. This attributes are the characteristics of continuous or normal grain growth [28, 29]. The distributions can be fitted by a log-normal one, with a correlation factor higher than 0.98, and present low asymmetry and dispersion. Mode and mean differ by less than 20 %, and over 90 % of all grains falls within the size range (0.5–2.5)*d/D*, inside the first confidence interval.

It is worth noting that static recrystallization could occur in the CAB samples because of extrusion stored energy. Recrystallization would lead to a fast growth of only few grains without appreciable growth of D. This because of the higher driving force compared with that for continuous grain growth [28]. Moreover, a bimodal grain size distribution, or at least a frequency increase of the lower d/D values tail, should be observed. However, the obtained grain size distributions do not show recrystallization signs.

Discussion

The first important result is the experimental verification of continuous grain growth. It is noteworthy that this behavior has been implicitly assumed, but no quantitatively evaluated for Cu-based SMA. The grain size distribution

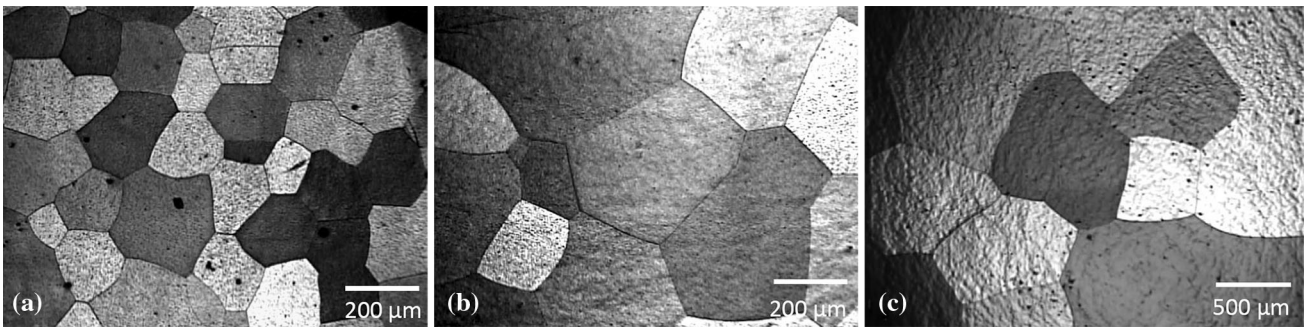

Fig. 3 Micrographs of CAB specimens after annealing treatment of 2 min at 1023 K (**a**), 10 min at 1023 K (**b**), and 10 min at 1123 K (**c**)

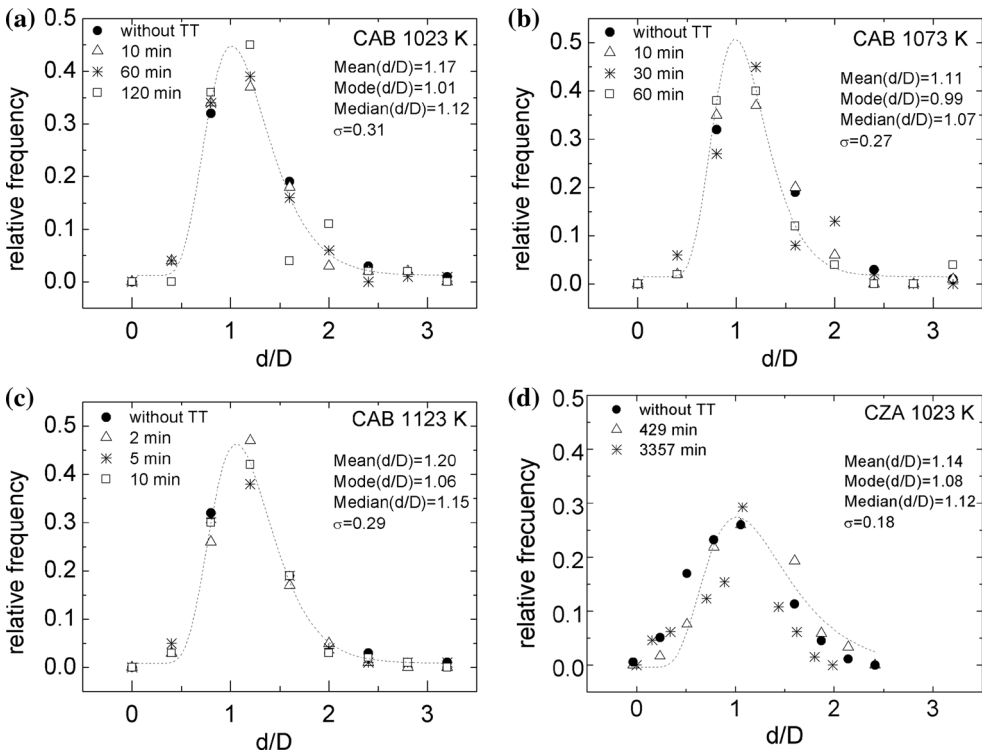

Fig. 4 Grain size distributions obtained for selected annealing times for CAB at 1023 K (**a**), 1073 K (**b**) and 1123 K (**c**), and for CZA at 1023 K (**d**)

normalized by the arithmetic mean grain size remains self-similar, with mode and mean at around the mean grain size D, plus low dispersion. The time invariability, and the highest frequency at around $d/D = 1$, guarantees D as a parameter which actually describes the microstructure along the annealing time. Abnormal grain growth would imply the development of an inhomogeneous microstructure, with grain sizes significantly scattered. The stress-induced martensitic transformation in Cu-based SMA has associated a significant shear deformation (up to 19 %) [30]. Such deformation in abnormal large grains implies great intergranular stress, and possible material disintegration. In this sense, a unimodal and narrow grain size distribution constitutes a suitable feature, particularly in view of possible stress-induced shape memory applications.

During aging, some grains grow while others shrink under the condition of volume conservation or area conservation, criterion valid in a 3D or 2D analysis, respectively. The growth rate of an individual grain of size d can be described by [31, 32]:

$$\frac{\mathrm{d}d}{\mathrm{d}t} = \alpha\gamma M\left(\frac{1}{D} - \frac{1}{d}\right), \tag{1}$$

where α is a constant ($1 \leq \alpha \leq 2$), γ is the interface tension, and M is the grain-boundary mobility. D is the instantaneous mean grain size, i.e., the critical grain size with zero growth rate under the requirement of area

conservation. Equation (1) indicates that the growing grains are that with $d > D$, and its growth rate is higher for higher d. From the grain diameter distributions of Fig. 4, we found that the percentage of growing grains is the (65 ± 5) % in the CAB, and the (50 ± 6) % in the CZA.

Assuming grain growth driven by boundary curvature, a growth rate equation for the average grain size can be written as [31]:

$$\frac{dD}{dt} = \frac{A}{D} \quad \Rightarrow \quad D^2 - D_0^2 = 2At \tag{2}$$

with D_0 the initial mean grain size, and A a parameter containing ($\alpha\gamma M$), temperature, and material dependent. This parabolic law is extensively used, although a generalized form with other grain growth exponent values, $n \neq 2$, are reported in order to improve the fit of the experimental data.

Figure 5 shows Eq. (2) applied to our results. An early departure from the ideal linear behavior is observed for the three temperatures, with a grain growth slowing transition earlier as the annealing temperature decreases. Once again, the lower annealing temperature dependence of the CAB grain growth compared with that of the CZA is reflected. Like in Fig. 2, but more evident, it is seen that grain coarsening almost ceases after long-time annealing, and a maximum average grain size is reached. Equation (2) supposes absence of pinning or drag forces, and deviations from its prediction can be considered as an indication of restrained grain growth. Actually, still with exponent $n > 2$, reflecting slow grain growth kinetics, Eq. (2) cannot fit the measured grain-growth curves over the entire range of annealing times in a large variety of materials.

The decrease in the grain growth rate with the increase of the grain size can be analyzed in terms of the driving force. The grain size increase leads to a decrease of the grain boundary area per unit volume, $\propto D^{-1}$, decreasing the grain boundary interfacial energy, and therefore decreasing the driving force for the grain growth. However, as we found, that unique process cannot describe the results. There are many grain-growth stagnation mechanisms proposed [28], such as pinning by second phase particles (Zener drag), order, triple junctions, solute drag, sample thickness effect, texture evolution, and smooth-boundary pinning.

The studied alloys are single-phase, with no inclusions, and annealing proceeds in the disordered state field of β-phase. Consequently, there are stagnation mechanisms which clearly do not operate, such as Zener drag and ordering.

It has been observed in SMA CuAlMn sheets that grain growth stagnation occurs by thermal grooving of grain boundaries at surfaces, and the limiting grain size, measured in the cross-section, is about two times larger than the sheet thickness [33]. This effect is described in [28]. In our case, the ratio maximum grain size/disk thickness is also around two in both alloys. We have performed annealing studies on cylindrical specimens of the CAB alloy, with 10 mm length and 3.5 mm diameter bars. The grain size measurements were made on the longitudinal and transversal faces. The results do not show remarkable differences with that here shown obtained for sheets. This suggests that surface effects are not crucial on the grain growth process in our case.

Departure from the $t^{1/2}$ grain growth law can be a consequence of texture development. Grain growth can leads to prominent changes of texture, with changes in the grain boundary energy and mobility. According to [34, 35], texture changes during grain growth has a kind of oscillating character. The grain size distribution widens, and grain growth is accelerated, when strong texture changes occur. This produces temporary broadening of the grain size distribution, and a stepwise grain size-t curve. The grain size distributions we obtained show an almost constant width along the annealing time (Fig. 4), and the grain coarsening rate changes seems to occurs continuously (Figs. 2, 5). Then, our results give no evidence of grain stagnation due to texture changes as main mechanism. Moreover, the martensitic transformation characteristics, highly dependent on crystallographic orientation, do not

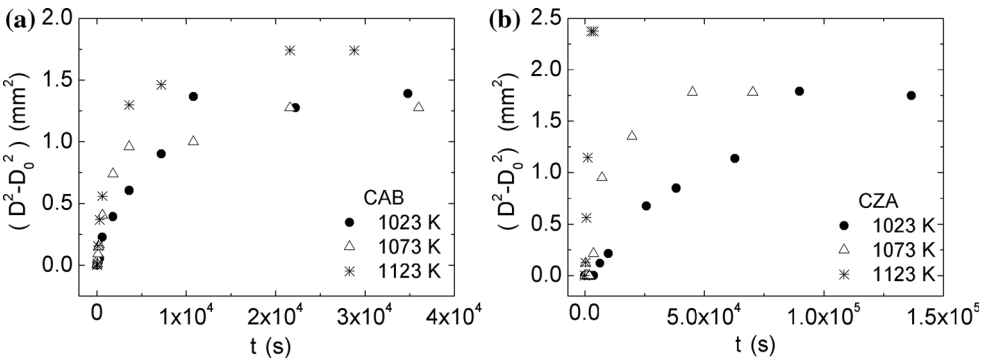

Fig. 5 Evolution of $(D^2–D_0^2)$ with the annealing time for the alloys CAB (**a**) and CZA (**b**)

reflect marked texture changes when measured as a function of grain size [10, 21].

Triple junctions can play an important role in the grain growth kinetics. However, its influence is expected in a reduced length scale, i.e., for ultrafine grain sizes [36].

More recently, it has been proposed the grain boundary smoothening mechanism [37]. With the thermal-activated transition from rough to smooth boundaries, the grain growth slows severely. Fractions of smooth boundaries can pin the complete interconnected network of grain boundaries, achieving a final stage of null grain growth rate. No explicit equations are proposed by Holm et al. [37], but simulations produce D–$t^{1/2}$ curves similar to that of Fig. 5 at high homologous temperatures, around $0.8T/T_m$ and higher. Then, this mechanism cannot be rejected.

Another important mechanism to consider is solute-drag (or impurity-drag). It is known that grain-boundary mobility is reduced by grain-boundary excess of solute (impurity) atoms, still in small amounts [38, 39]. The migration velocity of grain boundaries would not be linearly proportional to the driving force if solute is segregated to grain boundaries, which depends on the migration velocity, atomic diffusivity, and the concentration of segregation. Even though the theories explain the experimental observations, the derivation of a grain-growth law from this theory is not direct. Simulations results show that grain boundary segments with high impurity concentrations and low mobility are able to reduce the kinetics of the grain ensemble coarsening [40]. Moreover, boundary roughness decreases when the impurity concentration on the boundary increases, resembling the smooth-boundary pinning mechanism.

Solute atoms (Al, Be, and Zn) in the CAB and CZA alloys occupy the lattice sites with equal probability in the A2 state [30], and no segregation to grain boundaries is expected to occurs. However, alloys always contain impurities, still that laboratory-made. Considering that impurity levels as low as ppm lead to grain-growth stagnation in a variety of materials [38], the impurity-drag mechanism deserves particular consideration in this case.

Michels et al. [41] discuss in detail the drag influence on the grain-growth rate, and propose a modification of the differential form of Hillert's Eq. (2) incorporating a dragging force. Two types of dragging forces are considered, a constant force, Eq. (3), and a grain size (time) dependent force, Eq. (4):

$$\frac{\mathrm{d}D}{\mathrm{d}t} = A\left(\frac{1}{D} - \frac{1}{D_{\max}}\right) \tag{3}$$

$$\frac{\mathrm{d}D}{\mathrm{d}t} = A\left(\frac{1}{D} - \frac{D}{D_{\max}^2}\right), \tag{4}$$

where $D_{\max}$ is a maximum, limiting average grain size. Both equations predict a vanishing growth rate when D reaches the maximum value, for long annealing time. A constant retarding force is compatible with fixed obstacles, like the Zener drag effect by second-phase particles. A grain size dependent force is proposed for systems in chemical nonequilibrium, where solute (impurity) diffusion to grain boundary is promoted in order to reach a steady-state distribution. As is shown in [41], the resultant D–t curves from Eqs. (3, 4) are similar, however, according to the preceding discussion, the time-dependent drag-force equation is applicable in this case. The integral form of Eq. (4) leads to an equation with the form:

$$D^2(t) = D_{\max}^2 - \left(D_{\max}^2 - D_0^2\right)\exp\left(-2At/D_{\max}^2\right) \tag{5}$$

The experimental data fitted with Eq. (5) are shown in Fig. 6. $D_{\max}$ values were taken from Fig. 5. It can be seen that the fit is in reasonable agreement with experimental data.

The exponential parameter $\tau = D_{\max}^2/2A$ can be considered as a characteristic grain growth time, and it is shown in Fig. 7 as a function of the annealing temperature. It can be seen that τ is strongly temperature dependent in the CZA, while is weakly in the CAB. Since grain growth is a diffusion-controlled process, the τ temperature dependence is compatible with the lower vacancy migration energy in the CZA alloy, $\approx$0.65 eV [42], compared with that in the CAB alloy, $\approx$1 eV in [9].

The two terms in the growth rate, Eq. (4), the ideal growth rate A/D and the retarding term $AD/D_{\max}^2$, can be evaluated. Figure 8 shows the evolution of both terms with the average grain size for the CAB alloy. The retarding term is almost two orders of magnitude below than that of the ideal growth rate when $D \approx D_0$, that is at short annealing times. Despite the smallness of the dragging force, it is enough to produce the early departure from the ideal parabolic law (Fig. 5). The two growth rate terms equal earlier for the lower annealing temperature.

Our results can be compared with that reported by other authors for the binary CuZn and ternary Cu-based SMA. The evolution of the average grain size at 1073 K is shown in Fig. 9. Results of grain growth were taken from [22] for Cu–Zn (CZ), CuZnAl, and CuAlNi (CAN) alloys, and from [23] and [24] for CuZnAl. All those alloys were severely hot-worked before the annealing start.

The data reported in [22] and [23] have been analyzed according to Eq. (2), adjusting the grain growth exponent according to the annealing temperature. We have applied Eq. (5) to the D–t data, and the characteristic parameters are shown in Table 1. The experimental uncertainty from the fit in the τ determination is $\pm$20 % maximum. It is noteworthy that we do not find other reliable and compatible grain growth studies reported for ternary Cu-based SMA. Furthermore, $D_{\max}$ is only clearly reached and reported in [22], while longer annealing times are perhaps needed for the data

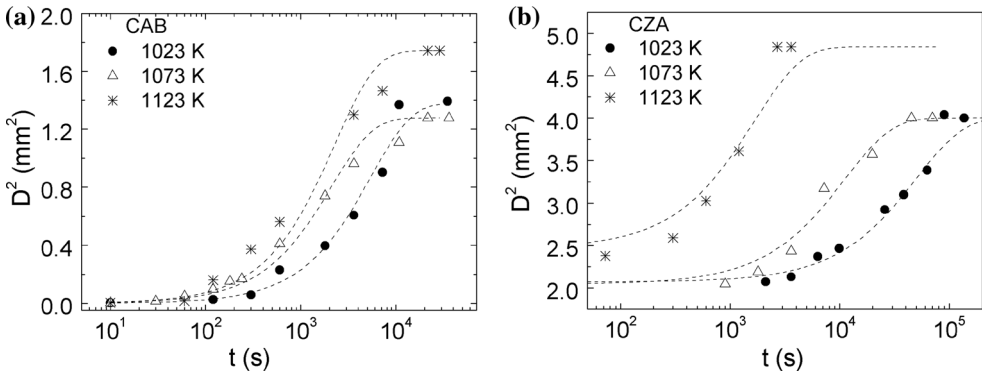

Fig. 6 Square mean grain size versus annealing time for the alloys CAB (**a**), and CZA (**b**), fitted by Eq. (5)

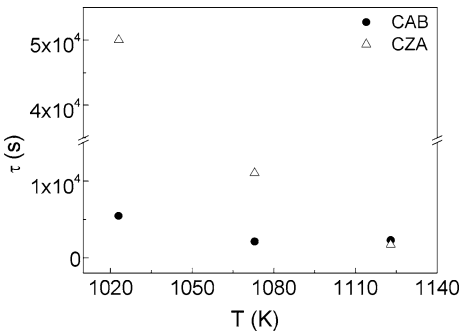

Fig. 7 Characteristic grain growth time versus annealing temperature

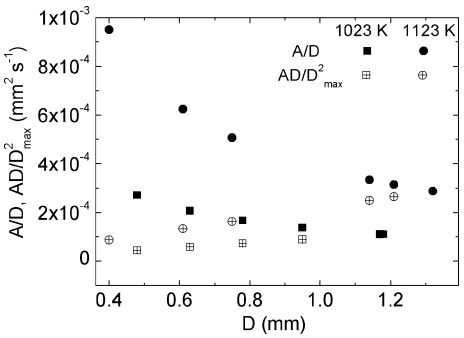

Fig. 8 Evolution of the growth rate terms of Eq. (4) with D for the CAB alloy

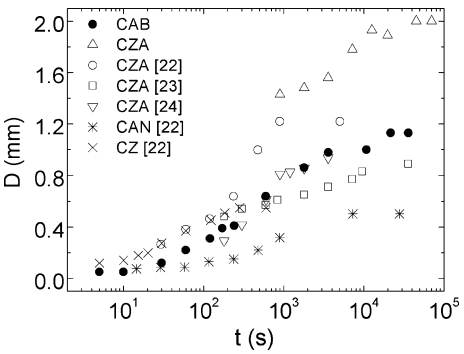

Fig. 9 Evolution of D with the annealing time at 1073 K for CAB, CZA, and reported data for other SMA. See text

Table 1 Initial grain size D_0, final grain size D_{max}, and the characteristic grain growth time τ at 1073 K

Alloy	CAB	CZA	CAN	CZ
D_0, D_{max} (mm)	0.05, 1.10	1.4, 2.0	0.07, 0.50	0.12, 0.55
		0.3, 1.2		
		0.5, 0.9		
		0.2, 0.9		
τ (s)	2×10^3	1×10^4	2×10^3	1×10^2
		5×10^2		
		5×10^3		
		1×10^3		

First line our results, *second line* from [22], *third line* CZA from [23], *fourth line* CZA from [24]

in [23] and [24]. At first sight, it is interesting the dissimilar behavior of the four CZA alloys, reflected in the different initial grain sizes, and the scattered growth characteristic time. This is an indication of the strong influence of alloy fabrication. The CZA alloys were severely hot-worked in different ways, except that here studied. The large initial grain size in the CZA we fabricate could be attributed to grain size increase during the homogenization treatment, and then we measured the final stage of grain growth during annealing. However, as can be seen in Table 1, the total grain size change during annealing is inside the range of grain size change of the four alloys, $0.4 \leq D_{max} - D_0 \leq 0.9$. As a general trend, ternary alloys exhibit higher characteristic growth time than the CZ one. This denotes that a slower grain growth occurs in ternary alloys.

Conclusions

The grain growth kinetics in two SMA, CuAlBe and CuZnAl, was studied in detail. The samples were subjected to isothermal treatments at 1023, 1073, and 1123 K.

The grain size distribution was determined as a function of time. The size distributions are time-invariant, which is

characteristic of normal grain growth. They can be fitted by a log-normal type relationship with low asymmetry and dispersion. It was verified that the arithmetic mean grain size is a parameter which really describes the microstructure along the annealing time.

The growth kinetics is strongly dependent on the aging temperature in CuZnAl, while is weakly in CuAlBe. It was verified that the grain size-time power law usually applied is not appropriate to describe the process, an early departure from the ideal behavior is observed, with a grain growth slowing transition earlier as the annealing temperature decreases. A modification to the grain size-time relationship was used, introducing a time-dependent dragging force, giving a reasonable approximation to the grain growth kinetics. The retarding term is almost two orders of magnitude below than that of the ideal growth rate at short annealing times. However, it is enough to produce the early departure from the ideal parabolic law. The obtained results were compared with that reported for CuZn and ternary Cu-based SMA. Higher characteristic growth times were determined for the ternary alloys.

Acknowledgements This work was supported by CONICET, ANPCYT, SECAT-UNCentro, and CICPBA, Argentina.

References

1. Van Humbeeck J, Kustov S (2005) Active and passive damping of noise and vibrations through shape memory alloys: applications and mechanisms. Smart Mater Struct 14:S171–S185
2. Otsuka K, Wayman CM (1999) Shape memory material, 1st edn. Cambridge University Press, New York
3. Van Humbeeck J (2003) Damping capacity of thermoelastic martensite in shape memory alloys. J Alloys Compd 355:58–64
4. Isalgue A, Fernandez J, Torra V, Lovey FC (2006) Conditioning treatments of Cu-Al-Be shape memory alloys for dampers. Mater Sci Eng A 438–440:1085–1088
5. Montecinos S, Cuniberti A (2009) Aplicación de aleaciones con memoria de forma CuAlBe en amortiguamiento pasivo de estructuras civiles. Rev SAM 6(3):20–29
6. Wang J, Wang Y, Schaublin R, Abromeit C, Gotthardt R (2006) The effect of point defects on the martensitic phase transformation. Mater Sci Eng A 438–440:102–108
7. Gröger R, Lookman T, Saxena A (2008) Distribution of the order parameter below Tc for a dislocation-free medium. Phys Rev B 78:184101
8. Lovey FC, Torra V (1999) Shape memory in Cu-based alloys: phenomenological behavior at the mesoscale level and interaction of martensitic transformation with structural defects in Cu-Zn-Al. Prog Mater Sci 44:189–289
9. Somoza A, Romero R, Ll Mañosa, Planes A (1999) Aging behavior in Cu-Al-Be shape memory alloy. J Appl Phys 85:130–133
10. Montecinos S, Cuniberti A, Romero R (2011) Effect of grain size on the stress-temperature relationship in a β CuAlBe shape memory alloy. Intermetallics 19:35–38
11. Montecinos S, Cuniberti A (2008) Thermomechanical behavior of a CuAlBe shape memory alloy. J Alloys Compd 457:332–336
12. Paradkar AG, Kamat SV, Gogia AK, Kashyap BP (2009) On the validity of Hall–Petch equation for single-phase β Ti-Al-Nb alloys undergoing stress-induced martensitic transformation. Mater Sci Eng A 520:168–173
13. Khan AQ, Brabers MJ, Delaey L (1974) The Hall-Petch relationship in copper-based martensites. Mater Sci Eng 15:263–274
14. Huang X, Wu DT, Zhao D, Ramirez AG (2013) Strengthening metals by narrowing grain size distributions in nickel-titanium thin films. J Mater Res 28:1289–1294
15. Ergen S, Uzun O, Yilmaz F, Kilicaslan MF (2013) Shape memory properties and microstructural evolution of rapidly solidified CuAlBe alloys. Mat Charact 80:92–97
16. Montecinos S, Cuniberti A, Sepúlveda A (2008) Grain size and pseudoelastic behaviour of a CuAlBe alloy. Mater Charact 59:117–123
17. Sutou Y, Omori T, Wang JJ, Kainuma R, Ishida K (2004) Characteristics of Cu-Al-Mn-based shape memory alloys and their applications. Mater Sci Eng A 378:278–282
18. Khan AQ (1974) The application and interpretation of the "time law" to the growth of β grain size and martensite plate thickness in copper-based martensites. J Mater Sci 9:1290–1296. doi:10.1007/BF00551846
19. White SM, Cook JM, Stobbs WM (1982) The grain size dependence of the loading and reversion behaviour of a Cu-Zn-Al MARMEM alloy deformed below M_f. J Phys-Paris 12:779–783
20. Arneodo Larochette P, Ahlers M (2003) Grain-size dependence of the two-way shape memory effect obtained by stabilisation in Cu-Zn-Al crystals. Mater Sci Eng A 361:249–257
21. Montecinos S, Cuniberti A (2014) Effects of grain size on plastic deformation in a β CuAlBe shape memory alloy. Mater Sci Eng A 600:176–180
22. Elst R, Van Humbeeck J, Delaey L (1985) Grain growth in β-copper-alloys. Z Metallkde 76:704–708
23. Wang FT, Chen FX, Wei ZG, Yang DZ (1991) The effects of microelements on the grain refining and the grain growth behaviors of CuZnAl shape memory alloy. Scr Metall Mater 25:2565–2570
24. Guilemany JM, Gil FJ (1991) Kinetic grain growth in Cu-Zn-Al shape memory alloys. J Mater Sci 26:4626–4630. doi:10.1007/BF00612397
25. Stipcich M, Romero R (1998) The effect of Ti-B on stabilization of Cu-Zn-Al martensite. Scr Mater 39:1199–1204
26. Lanzini F, Romero R, Stipcich M, Castro ML (2008) Long-range ordering in β-Cu-Zn-Al: experimental and theoretical study. Phys Rev B 77:134207
27. Montecinos S, Cuniberti A, Castro ML (2010) Kinetics of isothermal decomposition in polycrystalline β CuAlBe alloys. Intermetallics 18:36–41
28. Gottstein G, Shvindlerman LS (1999) Grain boundary migration in metals, 1st edn. CRC Press LLC, Florida
29. Atkinson HV (1988) Theories of normal grain growth in pure single phase systems. Acta Metall 36:469–491
30. Ahlers M (1986) Martensite and equilibrium phases in Cu-Zn and Cu-Zn-Al alloys. Prog Mat Sc 30:135–186
31. Hillert M (1965) On the theory of normal and abnormal grain growth. Acta Metall 13:227–238
32. Rios PR (1990) Effect of size distribution on the kinetics of normal grain growth and of particle coarsening. Acta Metall 38:2017–2021
33. Kusama T, Omori T, Saito T, Ohnuma I, Ishida K, Kainuma R (2013) Two- and three-dimensional grain growth in the Cu-Al-Mn shape memory alloy. Mater Trans 54:2044–2048
34. Abbruzzese G, Lucke K (1986) A theory of texture controlled grain growth-I. Derivation and general discussion of the model. Acta Metall 34:905–914
35. Eichelkraut H, Abbruzzese G, Lucke K (1988) A theory of texture controlled grain growth-II. Numerical and analytical

treatment of grain growth in the presence of two texture components. Acta Metall 36:55–68
36. Gottstein G, Shvindlerman LS, Zhao B (2010) Thermodynamics and kinetics of grain boundary triple junctions in metals: recent developments. Scr Mater 62:914–917
37. Holm EA, Foiles SM (2010) How grain growth stops: a mechanism for grain-growth stagnation in pure materials. Science 328:1138–1141
38. Cahn JW (1962) The impurity-drag effect in grain boundary motion. Acta Metall 10:789–798
39. Hillert M, Sundman B (1976) A treatment of the solute drag on moving grain boundaries and phase interfaces in binary alloys. Acta Metall 24:731–743
40. Mendelev MI, Srolovitzy DJ (2001) Grain-boundary migration in the presence of diffusing impurities: simulations and analytical models. Phil Mag A 81:2243–2269
41. Michels A, Krill CE, Ehrhardt H, Birringer R, Wu DT (1999) Modelling the influence of grain-size-dependent solute drag on the kinetics of grain growth in nanocrystalline materials. Acta Mater 47:2143–2152
42. Van Humbeeck J, Segers D, Delaey L (1985) The stabilization of martensite of step quenched CuZnAl martensite-Part III. Scr Metall 19:477–480